Chapter II

Methods

RESUMEN

Se han usado dos técnicas distintas para la medida de aberraciones totales y corneales.

Para la medida de aberraciones totales se ha desarrollado una nueva generación de la técnica de trazado de rayos laser —técnica creada originariamente en el Instituto de Óptica—. Diversas calibraciones y medidas sobre ojos artificiales muestran la precisión y repetibilidad de la técnica de trazado de rayos laser (valor medio de 0.063 μm en la repetibilidad en los coeficientes de aberración de onda).

Se ha desarrollado una técnica basada en la medida de la superficie corneal para la estimación de las aberraciones corneales. La medida de la superficie corneal se realiza mediante un topógrafo corneal basado en anillos de Placido. Los datos de elevación medidos por el topógrafo se interpolan mediante un desarrollo funcional, y posteriormente se obtiene la aberración de onda mediante una marcha de rayos virtual en un programa de diseño óptico. El error estándar (valor medio de los coeficientes de aberración de onda) debido a la precisión (0.013 μm) es del mismo orden que el error debido a la repetibilidad (0.015 μm).

Además de para la estimación de las aberraciones corneales a partir de los mapas de elevación corneal, la marcha de rayos virtual se ha utilizado sobre distintos modelos de ojo para el análisis de configuraciones que pueden ayudar a la comprensión de la interacción de aberraciones entre los distintos componentes oculares.

ABSTRACT

Two different techniques have been used to measure total and corneal aberrations.

A new generation of a laser ray tracing technique —originally developed in the Instituto de Óptica— has been implemented. Different calibrations and measurements on artificial eyes show the accuracy and precision of the technique (and average precision error of 0.063 µm in wave aberration errors).

The technique to estimate corneal aberrations is based on measuring the corneal surface shape. A Placido disk videokeratoscope is used to measure elevation data of the anterior corneal shape. Elevation data are interpolated by a functional expansion, and then the wave aberration is obtained performing a virtual ray tracing using an optical design program. The standard error (average value in wave aberration coefficients) due to accuracy (0.013 µm) is of the same order than that due to precision (0.015 µm).

In addition to experimental measurement of aberrations, virtual ray tracing on eye models has been used to analyze configurations where it is important to understand the optical interactions between different ocular elements.

1. Measurement of total aberrations

1.1 Laser Ray Tracing technique

A Laser Ray Tracing (LRT) technique is used to measure total aberrations of the human eye. The LRT technique was first implemented at the Instituto de Optica (CSIC) in 1997[1]. During this thesis a new generation of LRT has been developed, which incorporates improved capabilities over the previous version of the instrument [1-3].
Figure II.1 shows a schematic diagram of the second generation LRT, to whose development the author of the thesis has contributed.

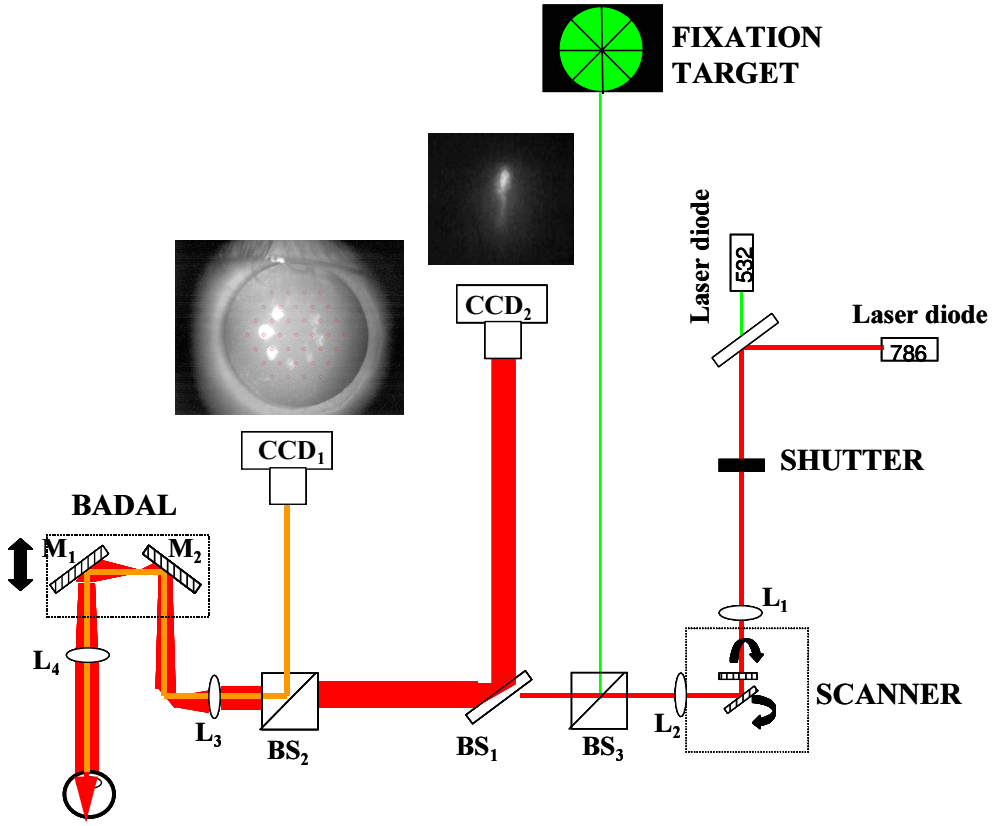

Figure II.1: Schematic diagram of 2nd generation Laser Ray Tracing. Light source is either a green (532 nm) or infrared (786 nm) laser diode. The beam is focused and collimated by lenses L_1 and L_2. An x-y scanner system (at the focal point of L_2) deflects the rays. A Badal system (formed by lenses L_3, L_4 and mirrors M_1 and M_2) corrects for the eye's spherical refractive error. The light reflected back from the retina passes through the Badal system again, and is projected on the high resolution camera CCD_2. Another camera (CCD_1), coaxial with the system, collects simultaneously images of the pupil and is used for continuous alignment. A fixation target displayed on a LRT monitor is also viewed through the correcting system.

In this system laser rays sample the eye's pupil sequentially. The laser sources are a green He-Ne laser, 543 nm (which was used in the studies presented in chapters III, IV, V) and an infrared (786 nm) diode laser coupled to an optical fiber (chapter VI, VII). Studies in our laboratory[4] have shown that there are not significant differences in the aberrations measured in visible or infrared light, except for the defocus term.

A scanning system formed by two mirrors (X-Y) deflects the laser beam at various angles. A set of parallel beams is then achieved by a collimating lens (L2), located at one focal distance from the scanner. The astigmatism induced by the physical separation of the mirrors is compensated by a cylindrical lens. The scanner system is automatically controlled, and can be configured to sample the pupil with different sampling patterns and densities. In this thesis we typically use a hexagonal sampling pattern of 37 points with a step size of 1 mm, and pupil size of 6 mm. The sampling beam diameter is 0.5 mm, and therefore an effective pupil of 6.5 mm is considered in the computations. In some of the studies, however, the sampled pupil was reduced. For example in elderly eyes –chapter VII-, where dilated pupils were typically smaller, or in patients with contact lenses with smaller diameters. In those cases, the step size was appropriately reduced.

The number of samples that we used allows a 7^{th} order polynomial fit of the wave aberration (with 35 terms). Several studies [5, 6] have shown that a larger number of samples is not necessary to retrieve ocular wave aberrations.

A high resolution, cooled CCD_2 camera, conjugate to the retina records a series of aerial images reflected from the retina, as the laser beam samples the pupil. A set of background images is recorded with the same conditions but using a black diffuser in front of the eye.

By the effect of aberrations, the retinal spot moves as the entry location moves. The second pass only affects the spot image shape but not its location. Centroids of the aerial images are evaluated using image processing. Firstly, background images are subtracted from raw images. A filtering and thresholding is applied on the images to avoid intensity noise due to scattering. Finally, centroids are evaluated as computed intensity mass center of the treated images. Figure II.2 shows how the centroid is evaluated on an aerial image. In the second generation the images sizes captured by the CCD_2 are 256x256 pixels frames with a field angle subtended of 1.27 arcmin per píxel.

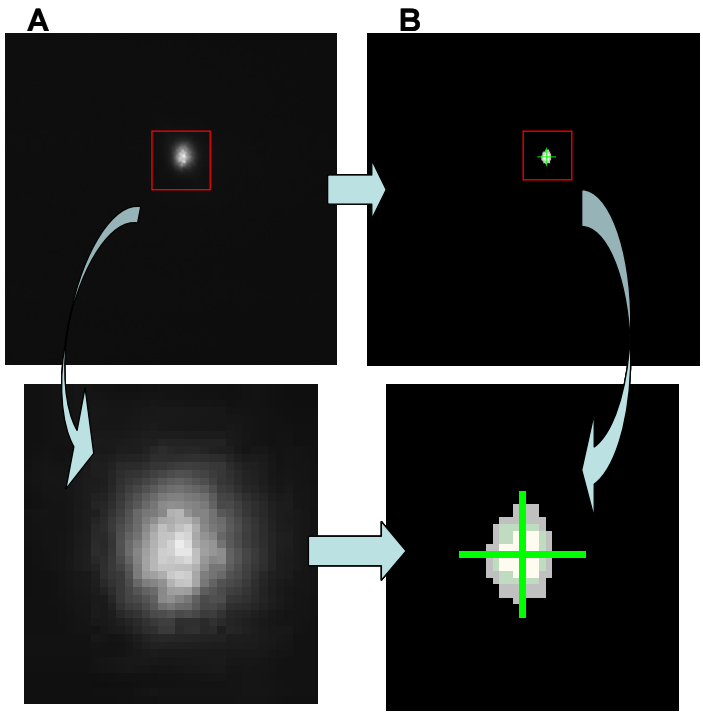

Figure II.2: A) Image frame (256x256) corresponding to a recorded aerial image. **B)** Image processing of raw image A. After subtracting the background image, filtering and thresholding, the centroid is computed as an intensity mass center. The computed centroid is marked by the green cross over the spot.

Transverse aberrations are computed as the difference of the aerial image centroid location with respect to the centroid of the image corresponding to the beam passing through the pupil center (chief ray). Transverse aberrations are the slopes of the wave aberration with a scale factor[7]. From this set of discrete slope values, a modal reconstruction, following a least squares method, of the global function for the wave aberration is used. The wave aberration is described by a 7^{th} order Zernike polynomial expansion (see section 1.3 in Introduction).

While the system can measure transverse aberrations corresponding to a defocus up to ±6 D, refractive errors were typically compensated by means of trial lenses (in the first generation of the instrument) or a Badal optometer (in the second generation, mirrors M1 and M2, and lenses L3 and L4 in Figure II.1). Trial lenses were placed in front of the subject's eye, and magnification factors of the pupil sampling were compensated by software. The Badal system compensated for the refractive errors without modifying the sampling pattern. The effect of the compensation of the refractive error on the measured aberrations was studied experimentally and computationally. We performed

experimental measurements of aberrations in an individual myopic eye (-6 D) with different amounts of correction with trial lenses (-6D and -3 D). The sampling effects were corrected by software, and therefore the analysis relates to the effects of convergence. Additionally we performed simulations in an optical design program (Zemax) using an eye model (see Table II.1) with simulated trial lens located 20 mm in front of model cornea (-3 and -6 D. The corneal topography of the control subject was used in the simulation. Simulations were performed with a standar model of the crystalline lens (see Table II.1). Differences are expected to affect predominantly thespherical aberration[8]. Computer simulations showed a slight change of spherical aberration. It increased (with respect to the uncorrected eye) by 0.043 µm with a -3 D trial lens and by 0.111 µm with a -6 D trial lens. The experimental differences were smaller: 0.066 µm with a -3D trial lens and 0.018 µm with a -6D trial lens. Therefore, no trend with increasing trial lens power was found experimentally and the differences found are within the experimental error. Calibrations of the system were performed using trial lenses (both spherical and cylindrical) as well as phase-plates of known aberrations.

The line of sight (i.e. foveal fixation and pupil center) was used as a reference axis. A video camera conjugate with the pupil plane is used to monitor eye alignment with respect to the optical axis of the instrument. A fixation channel (a laser spot in the first generation of the instrument, and a cross-pattern generated in a CRT display in the second generation) provides a fixation target during the measurement.

Subjects' head were stabilized with a dental impression and a headrest, and the pupil was continuously monitored on a CCD camera. Each measure was repeated five times. Each series of images was obtained in 4 seconds (first version of the instrument) to 1.5 seconds (second generation of the instrument).

Laser light intensity is attenuated by neutral density filters to reduce the energy exposure at least one order of magnitude below safety levels of the American National Standard Institute for this wavelength[9]. In the second generation of LRT, for the 532 nm laser the power was (6.5 mm pupil) always less than 3.42 µW, and for the 786 nm laser the maximum power was 36.9 µW.

2. Virtual ray tracing and eye modeling

Virtual ray tracing with an optical design program, Zemax (10 April 2003, Focus Software, Tucson, AZ) has been extensively used in this thesis. In the following sections we provide basic concepts of the ray tracing procedures with this tool, as well as the particular applications for the studies conducted in this thesis.

2.1 Virtual ray tracing

Virtual ray tracing is based on geometrical optics principles. Ray tracing algorithms in optical design are based in two steps: The *translation step* that involves translation of one ray from one surface to the next one, and the *refraction step* that evaluates the refraction of a ray in a determined surface point. The translation step is solved by geometrical considerations determining intersections of lines (ray paths in an isotropic and homogeneous medium) and surfaces (lens surfaces), while the refraction step, if a real ray tracing is performed (i.e. no paraxial approximation), is calculated applying Snell´s law. In the case of not homogeneous medium (i.e. gradient-index) different algorithms for the translation step are used such as Sharma algorithm[10]; this method, used in Zemax, is based on Runge-Kutta method for solving the differential ray equation.

Several variables must be pre-defined for the ray tracing: 1) Position of the object point or, for objects at infinity, the field angle of the ray fan entering the optical system. 2) Position and shape of image surface (normally a plane). 3) Stop surface and size, which defines the entrance-exit pupil size and position. 4) Wavelength used for the ray tracing.

The wave aberration is computed directly from the ray tracing analysis: An aberration-free wavefront is described by a sphere of radius given by the focal length of the system. This sphere, called “reference sphere”, is first evaluated. A ray passing through a defined pupil position is refracted with a known direction as determined by ray tracing. Considering a single ray, let A be the position where this ray is located in the real wavefront. A is calculated by evaluating the distance, from the pupil through the refracted ray, equal to a defined distance in the optical axis (the wavefront is defined as the surface of equal phase or optical path). The wave aberration is the distance from point A along the refracted ray to the intersection with the reference sphere (see Figure I.1).

For each ray traced, a local value of the wave aberration is obtained. Therefore, a complete ray tracing procedure provides a discrete set of local measurements of the wave aberration. There are two ways of retrieving the wave aberration function from these discrete set: Zonal and modal reconstruction. Zonal reconstruction is based on numerical integration techniques. Modal reconstruction uses data fitting to a set of orthogonal functions. Zemax uses a modal reconstruction with a standard least squares algorithm fitting to a Zernike expansion.

2.2 Eye modeling using Zemax

For several purposes, such as optical testing or evaluation, eye modelling has been carried out using Zemax. To characterize an optical system, it is necessary to define a sequential group of "surfaces" separated by refractive index media. Depending of the application different types of "surfaces" have been used. Standard surfaces (defined by an apical radius and conicity) were used in some of the applications as simple models of the ocular surfaces. Grid sag surfaces, which allow a evaluation of the surface in a set of sampling points, were used to model surfaces measured with the videokeratographer. Gradient index surfaces (using C extension capabilities of Zemax) were used to construct GRIN lenses (chapter VIII).

The ocular media refractive index data used are based on anatomical data reported by Le Grand et al[11] with the update in the refractive index of the cornea of Escudero et al[12]. Index dependence of the wavelength is introduced fitting experimental longitudinal chromatic aberration[13] with Herzberger formula[14].

Table II.1 summarizes the details of the eye model and relevant parameters used in different studies of this thesis.

Study/ Chapter	Anterior corneal surface	Posterior corneal surface	Anterior lens	Posterior lens	Other
Effect of trial lens on measuring aberrations (chapter II)	Individual corneal surface	Conic surface with R=6.31, Q=0	Conic surface with R=10.2, Q=-3.13	Conic surface with R=-6, Q=-1	Gullstrand GRIN for the crystalline lens
Effect of beam convergence over internal aberrations estimation (chapter V)	Pre & Post LASIK individual corneal surfaces	Conic surface with R=6.5, Q=-0.26	Conic surface with R=10.2, Q=-3.13	Conic surface with R=-6, Q=-1	Corneal thickness: 0.5 mm. Anterior chamber depth: 3.05 mm. Lens thickness: 4.0 mm
Changes in the posterior cornea with LASIK (chapter V)	Pre & Post LASIK individual corneal surfaces	Pre & Post LASIK conic surfaces reported by Seitz et al[15]	N.A.	N.A.	Corneal thickness: 0.5 mm
Aberrations after cataract surgery. Comparison with in vivo measurements (chapter VII)	Individual corneal elevation surfaces	Conic surface with R=6.31, Q=-0.51	Manufacter IOL design data		Anterior Chamber depths and axial length measured by biometry
Theoretical aberrations of IOLs (chapter VII)	Ideal cornea with no aberrations		Manufacter IOL design data		Virtual point object to produce desired convergence
Effect of tilt & decentration with IOLs (chapter VII)	Ideal cornea with no aberrations		Manufacter IOL design data		Tilts and decentration from biometry data in the literature

Table II.1: Parameters used for the different eye models used in different studies of this thesis.

3. Measurement of corneal aberrations

There are three steps in evaluating corneal aberrations of the anterior corneal surface: 1) Obtaining experimental data with a videokeratoscope. 2) Modelling of the corneal surface from these data. 3) Evaluating corneal aberrations from the corneal model surface.

3.1 Videokeratoscope data

Corneal topography data were obtained with a Placido disk videokeratoscope (Humphrey-Zeiss MasterVue Atlas). Placido disk videokeratoscopes analyze specular reflection off of the cornea of a set of concentric illuminated rings (Placido disk) recorded by a video camera. The system has a central clear zone through which the subject views a

fixation target. From the image of the reflected rings an algorithm reconstructs the shape of the anterior corneal surface.

The reconstruction algorithm for the Humphrey-Zeiss topographer is referred to as *arc step algorithm*, and has been described in detail by Campbell[16]. This algorithm reduces the reconstruction to analyze the corneal surface in a set of meridian planes, "reconstruction planes", containing the videokeratoscope axis (VK axis). The VK axis is defined as the axis that intersects the image plane at the mean center of the inner rings reflections and passes through the center of the entrance pupil of the videokeratoscope[16]. The algorithm extracts corneal shape data in the reconstruction planes separately. This algorithm assumes that reflection rays in a meridional plane stay on the same plane. Rays not obeying this condition are named skew rays, and the error associated with this approximation is called *skew error*.

For each reconstruction plane, a meridional curve of the corneal surface is evaluated. These curves are fitted by small sections of circular arcs by an iterative algorithm obtaining the axial and radial positions and slope of the curve at different points.

The Placido disk is formed by 24 rings. There are 180 reconstruction planes with 2 degrees of angular distances among planes. Therefore for each reconstruction plane there are 48 evaluated points, and the total number of points in the global reconstruction is 48*180. However some of these data is lost because of tear film break up effects or eyelid oclusions. Figure II.3 shows the set of points where the corneal surface is evaluated for a real cornea.

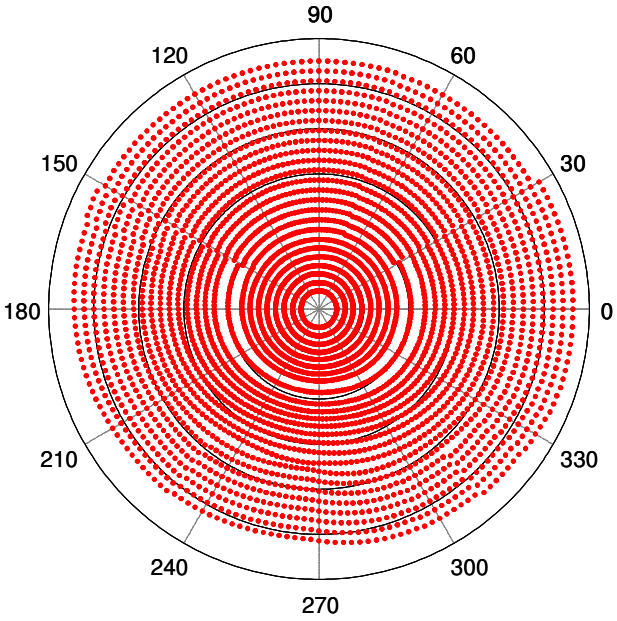

Figure II.3: Corneal polar coordinates where elevation data are given by the videokeratoscope.

3.2 Modelling the corneal surface

Corneal surface modelling is limited by the distribution of videokeratoscope data. As this distribution is not uniformly spatially sampled in XY coordinates, with no data between rings, and specially within the central clear zone (around 0.4 mm radius), strategies with local interpolations do not work properly. In general, a smooth global interpolation by polynomial expansion offers better results. Considering the circular symmetry of the data, the Zernike polynomial expansion appears to be a good choice[17a]. We fitted corneal surfaces with a Zernike polynomial expansion using 37 terms, and a standard least squares optimization by means of the inverse matrix built-in function given in Matlab. It has been noted that a finite and relatively small number of Zernike terms is sufficient to prevent fitting the noise error of the videokeratoscope by over-parameterization[19]. Schwiegerling et al[17] suggested the use of Gram-Schmidt othogonalization for a more stable numeric interpolation of the corneal data set of discrete points (Zernike polynomials is a orthogonal base only over a continuous range).

[a] Iskander et[18] al have proposed the use of an alternative set of polynomials referred to as Bathia- Wolf.

However, Salmon et al[20] reported that for the set of data provided by typical videokeratoscopes the convergence in the least squares procedure for the corneal modelling is not significantly different whether Gram-Schmidt orthogonalization is used or not.

Once the surface is modelled by Zernike polynomial expansion, discrete points are evaluated in a XY equi-space grid to be introduced in Zemax for the corneal ray tracing evaluation.

3.3 From corneal surface to corneal wave aberration

Using geometrical optics there are two main different ways of evaluating wave aberration from corneal surface data. These methods are based on two different, but equivalent, definitions of the wave aberration[21]. The first definition relies on the difference of the ray path between two points in the real and ideal wavefront for each pupil coordinate. In Figure II.4, this is indicated by the distance W. The second definition defines the wave aberration as the optical path difference between the chief ray and a marginal ray that passes through the surface at a point A. In the same figure, the optical path of the chief ray is $[OV]n + [VO_p']n'$ and that of the marginal: $[OA]n + [AO']n'$. Thus the wave aberration is $W=n[OA-OV] + n'[AO_p'-VO_p']$.

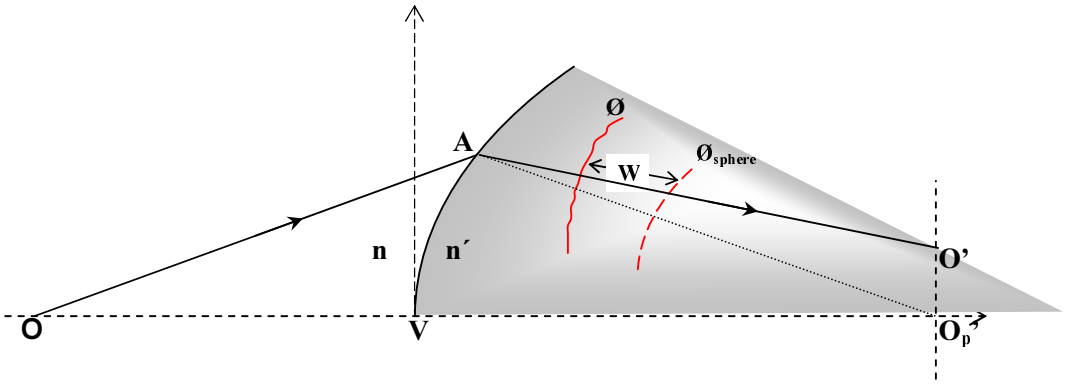

Figure II.4: Simplified scheme showing the differences across methods to evaluate corneal aberrations. [OA] and [AO'] show the path of a specific ray. O' is the intersection of the ray with the image plane. O_p' is the paraxial image point of O by the surface. Ø and $Ø_{sphere}$ are the real and ideal wavefront respectively. W indicates the wave aberration of the considered ray.

While the first method requires a ray tracing procedure to evaluate the real wavefront (normal surface of the refracted rays) the second method does not need a ray tracing because it does not use the O' intersection of the real ray with the image plane. To reduce complexity in the analytical solution of the second method it is necessary to use some approximations, such as series truncation of polynomial expansions, to reduce the amount of calculations [20-23]. A third method, as a variant of the second one, evaluates the wave aberration as the difference of the corneal shape from an ideal surface —Cartesian oval surface— for which wave aberration is zero[24, 25]. Salmon et al.[20] have evaluated the differences between the different methods and found that differences are about 1.3 % for conic corneal models between a ray tracing procedure and the optical path difference method.

For this thesis the exact ray tracing technique, evaluated with Zemax, is used as explained in section 2.1. The model surface is introduced in ZEMAX using a finite difference method to evaluate the normals to the surface —necessary to apply Snells' law—.

The ray tracing technique has been used in real corneas, to our knowledge, also by Sarver et al[26], based on Greivenkamp et al[27] work. Previous studies used paraxial ray tracing rather than real ray tracing[28].

3.4 Additional considerations in ray tracing through corneal surfaces

There are several details in the ray tracing routine to evaluate corneal aberrations that need to be discussed in detail.

Sampling of the ray tracing

The wave aberration is reconstructed from a finite number of rays. The accuracy of the result depends on whether the sampling is sufficiently dense. Because there is not a universal method to know how many rays are sufficient, a way to ensure the reconstruction is to evaluate the wave aberration for different number of rays for different corneal surfaces. Table II.2 shows RMS (3rd and higher) for different sampling densities in ray tracing on three real corneas.

Sampling Ray Tracing	32x32	64x64	128x128	256x256	512x512
Normal young corneal surface					
Comput. time (s)	~0.2	~1.0	~2.9	~13.8	~61
RMS (µm)	2.0411	2.0402	2.0411	2.0410	2.0410
Post LASIK corneal surface					
Comput. time (s)	~0.2	~0.9	~2.9	~12.7	~55
RMS (µm)	4.5006	4.4987	4.4988	4.4990	4.4989
Keratoconus corneal surface					
Comput. time (s)	~0.2	~0.98	~3.0	~12.5	~59
RMS (µm)	6.7402	6.7331	6.7477	6.7460	6.7455

Table II.2: Effects of sampling ray tracing in computing wave aberration of three different corneal surfaces. Pupil diameter used is 10 mm. Zernike expansion evaluated up to 45 terms. RMS of 3rd and higher aberrations for a 0.543 nm wavelength. Computations were done with a Pentium IV (1.7 GHz).

Table II.2 shows that the number of sampling rays to ensure a good wave aberration evaluation depends on the corneal surface. More aberrated corneas needed a higher number of rays. For the worst case of a highly aberrated cornea (keratoconus), the algorithm converges numerically for sampling densities above 128x128 to a difference of less than 0.0017 µm in the RMS. For higher densities computing time starts to become impractically large.

Pupil axial position

To evaluate corneal aberrations it is not only necessary to know the surface, but also the position of the "stop" surface that determines the position of the entrance pupil. In the case of the corneal surface the stop is the iris, and its actual position varies across subjects. We have evaluated that, in practice, we can suppose that the stop is situated in the corneal surface, and the error is, in general, negligible.

To quantify this error we calculated with Zemax corneal aberrations of a real eye, where the anterior chamber depth was measured (2.91 mm), with stop position located at the corneal surface or at the actual iris position (i.e. 2.91 mm behind the cornea). RMS of 3rd and higher was 1.2178 µm and 1.2179 µm respectively. Differences of individual

Zernike terms were also negligible, with the maximum difference being 0.00046 μm for term Z_4^{-4} (the most affected by this error).

Object position

Experimentally, we evaluate optical aberrations for unaccommodated eyes. Therefore, the object was always considered at infinity. Following this criterion, to evaluate corneal aberrations we placed the object at the infinity to achieve rays parallel to keratometric axis.

Reference "sphere": Image plane position

An aberrated wavefront changes its shape as it propagates, so the wave aberration depends on the radius of the reference sphere taken as ideal reference. For small aberrations, this is a small effect, but for large aberrations, it should be taken into account. In paraxial optics it is not difficult to find the ideal sphere —see definition in chapter I section 1.1—, but for irregular surfaces there is some uncertainty to define the ideal sphere. In order to provide a direct comparison with total aberrations the reference sphere must be chosen with a similar criterion. When measuring experimentally the ocular wave aberrations, the image plane is located at the retina, and typically found by assessing the eye's best subjective correction. When estimating corneal wave aberrations we use the best focus position as the position that minimizes the root-mean-square spot size. Alternative best focus definitions could be used, such as minimizing root-mean-square wavefront error. We found that differences across Zernike coefficients computed using both criteria were only in the third decimal digit for real corneas. There are even other definitions of the ideal sphere of an irregular surface. To our knowledge, the commercial software CTView developed by Sarver and Associates, Inc, evaluates the sphere radius as an average of reference radius for the set of corneal points, where in each point the sphere radius is obtained forcing a zero optical path difference with respect the chief ray.

Medium of refraction index: Tear film influence

The corneal surface separates two media: air and a second medium. For ray tracing, the index of refraction of this second medium is relevant.

The human cornea is composed by several layers. From the corneal surface to the

anterior chamber: Tear film, Epithelium, Bowman´s membrane, stroma, Decement's membrane and endothelium. Each of these layers has different thickness and refractive index. Therefore, for a realistic optical modeling of the cornea all these magnitudes should be accurately measured. However to date there is limited knowledge of the refractive index of the different layers —Patel et al[29] provides the following refractive indices: 1.401 for the corneal epithelium, 1.380 for the anterior stroma and 1.373 for the posterior stroma—. Some controversy exists in the assignation of an average refractive index for the cornea modeling, and in particular the evaluation of tear film contribution. In fact, the major refractive index change for rays entering the cornea occurs between air and tear film (tear film index is ~ 1.3367[30]). Albarrán et al[31] showed that, in paraxial approximation, the total refractive power of the cornea does not change whether the tear lens is considered or not. However, even a simple model which simulates the tear film as a meniscus (first surface convex and second surface concave) with conic surfaces, predicts that spherical aberration of tear film would play a role. It is easy to show that only very specific combinations of radius and asphericities could explain a spherical aberration-free tear film. When irregular surfaces are considered, contribution of the tear film to higher order aberrations is likely.

Some authors[20, 32, 33] have used an average value of refractive index of 1.376 to model the cornea, ignoring the tear film, while other authors[23, 24, 28] use an effective value of 1.3375, closer to consider the effect of the tear film.

In this thesis, considering the lack of information of the real refractive structure of the cornea, we reduce it as a thin lens which separates two media: Air and aqueous humour, n=1.3391 for a 0.543 μm wavelength, which is a value close to the effective value (1.3375) used for modelling the whole cornea.

Referring corneal wave aberration to the line of sight axis

While the total aberration measurements with the LRT system are referred to the line of sight, the videokeratoscope uses the keratometric axis for centration (passing through the fixation point and center of curvature of the cornea). These two axes intersect the entrance pupil at different locations and differ by an angle β. A schematic diagram is shown in Figure II.5.

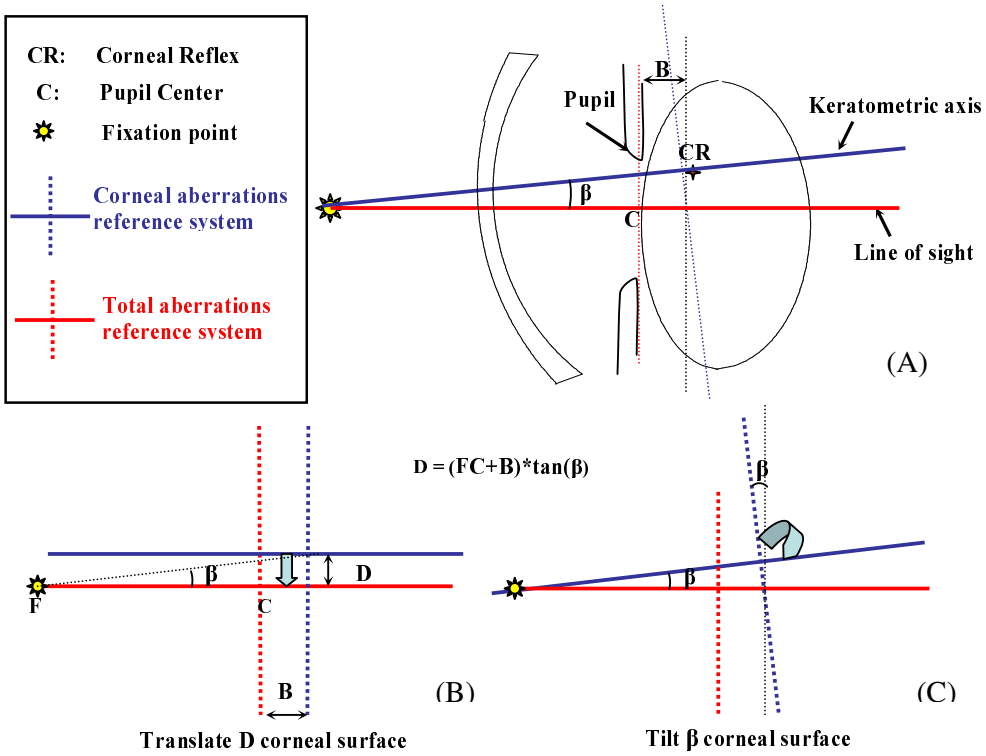

Figure II.5: (A) Total aberrations are referred to the line of sight and measured at the pupil plane. Corneal topography is referred to the keratometric axis and it is measured at the plane normal to the keratometric axis at the corneal reflex. **(B)** Both reference systems and shifted by distance D, which is corrected with the recentration algorithm. **(C)** Reference systems are also tilted by angle β.

The difference between the two reference systems can be decomposed in a shift difference —distance D— and a tilt —angle β—. Since the entrance pupil center is not available from the Humphrey-Zeiss videokeratoscope pupil images, due to the superposition of the Placido rings with the pupil margin, we have developed a custom software to correct for the shift (D) between corneal aberration and the total wave aberration map. The routine finds the pupil position that produces a minimum in the difference of corneal to total aberrations. Corneal aberrations are computed over a large pupil diameter (10 mm) and re-computed over a smaller pupil (matching the pupil size of total aberration measurements), moving the center across a 1-mm square region around the position of the corneal reflex, at 0.1-mm steps. A difference total-corneal map is computed for each pupil location, and the RMS of the difference map is calculated. This surface shows a minimum, typically slightly off-center from the corneal reflex. Figure II.6 shows several examples of RMS difference maps.

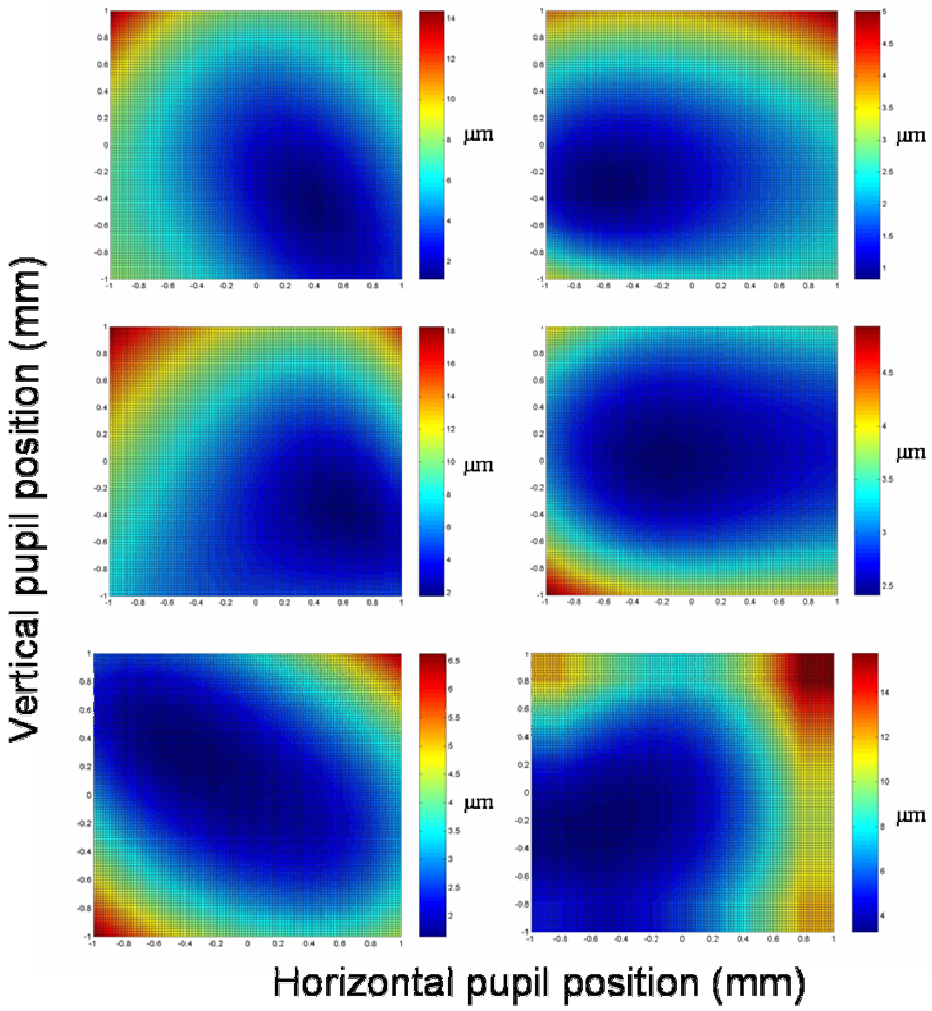

Figure II.6: Examples of RMS difference maps between total a corneal wave aberration maps. Pupil coordinates are referred to corneal reflex. Blue colors indicate regions where RMS is lower.

In all cases the location of the minimum is well defined. The procedure is typically done considering 3rd and higher order aberrations in both the total and corneal aberration maps. Independent measurements of the relative displacement of the 1st Purkinje image with respect to the pupil center on selected subjects [34] showed similar results than those retrieved by the described procedure.

We computed that for a typical eye corneal aberration data (3rd order and higher) changed by 10% when shift D was corrected. While, as expected, spherical aberration did not change significantly by the centering procedure (3% on average), third-order aberrations changed by 22%. Figure II.7 shows the corneal aberration pattern for the same eye, centered at the corneal reflex (as directly processed from the corneal

videokeratoscope raw data) and at the pupil center. While direct corneal data show no coma, when the actual pupil position is taken into account, we observed that coma is predominant along with spherical aberration.

The routines described above correct for the shift distance D, but do not correct for tilt by the mentioned angle β. This angle can be computed by measuring the distance between the anterior corneal intersects of both axes, taking into account the fixation point distance for this instrument. While the keratometric axis intersection with the anterior corneal surface could be located by means of the corneal reflex, the corneal sighting center (intersection of line of sight with anterior corneal surface) is not available in our patients. Mandell et al[35] reported an average difference of 0.38±0.10 mm between the corneal intersect of the keratometric axis and corneal sighting center across 20 normal eyes. Assuming similar values in the eyes measured in this thesis, and for the nominal 148.3-mm fixation point distance in the Humprhey-Zeiss videokeratoscope, the angle β (angle between keratometric axis and line of sight) is ~0.15 deg. Taking this average tilt into account, RMS changes only by 3.1% for 3rd order terms, and 0.43% for spherical aberration.

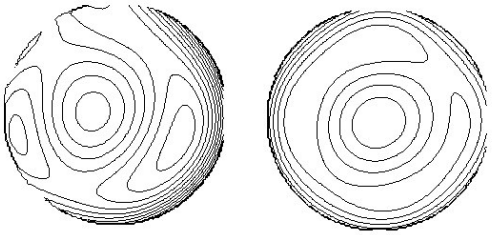

Reference: pupil center Reference: corneal reflex

Figure II.7: Corneal wave aberration contour maps for a corneal surface, after LASIK surgery, centered at the pupil center, after realignment (*left*) and centered at the corneal reflex (*right*), directly from corneal topography data without realignment. Contour line spacing: 1 µm. Pupil diameter: 6.5 mm. Piston, tilt, defocus, and astigmatism excluded to minimize the RMS wavefront error in each map.

4. Internal aberrations estimation

Wave aberrations of a multi-element system are additive[21], thus wave aberration of the total eye can be treated as the sum of corneal and internal aberrations. However it should be considered that in this scheme, while the wave aberration for the cornea is evaluated for an object point situated at infinity (parallel incoming rays), for the crystalline lens the wave aberration is evaluated with respect an object point O' (Figure II.8), being O' the cornea focus point. The position of the virtual object O' with respect to the lens is the focal length of cornea surface minus the length of the anterior chamber as shown in Figure II.8.

For a typical corneal focal length of 30 mm and an anterior chamber depth of 3 mm, when corneal aberrations are subtracted from total aberrations, the aberrations of the crystalline are expressed for a virtual object point situated at (cornea F' – ACD)=30 mm-3 mm=27 mm from the back surface of the crystalline lens. Furthermore, the virtual object point is not a perfect point because of the aberrations of the cornea, although the effects of wave aberration of the incoming beam into the lens are less critical than the global convergence.

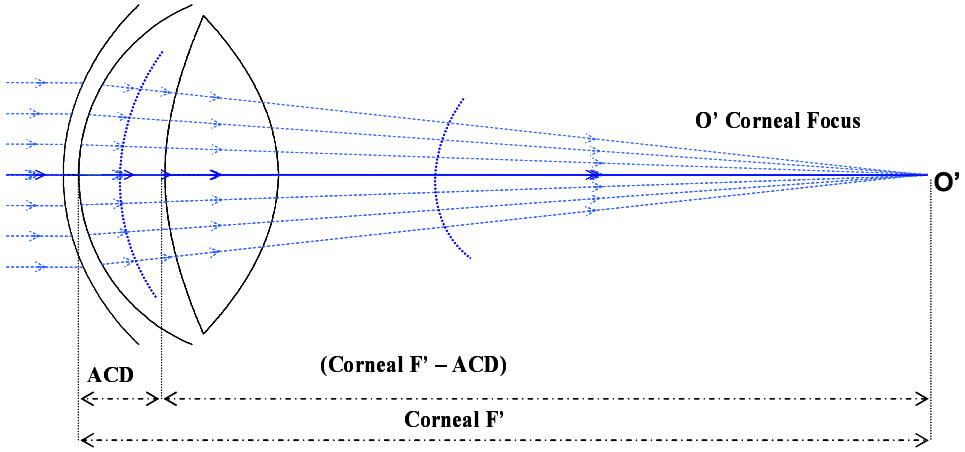

Figure II.8: Virtual ray tracing through a schematic eye model. The refracted rays are only shown after passing through the cornea converging to the best corneal focus point. This point is the virtual object point for the crystalline, at a distance given by the corneal focus minus the anterior chamber depth (ACD), from the back vertex of the first surface of the crystalline lens.

Therefore, apart from the aberrations of the crystalline lens (or intraocular lens in patients after cataract surgery), internal aberrations also contain the effects of the convergence of the incoming beam, and therefore will be affected by anterior corneal shape and the individual anterior chamber depth, as well as the posterior surface of the cornea. Possible influence of the posterior corneal surface on the measured internal aberrations will be discussed in chapter IV and V. We will also study possible changes in internal aberration measurements with changes in anterior corneal shape (such as occurs with LASIK in chapter V).

5. Accuracy and precision: source of errors

Measurement errors are usually classified under two different categories: ***Bias errors*** and ***Precision errors***. ***Bias errors*** are those systematic errors related to the nature of the measurement and are expected to be constant across measurements, affecting the ***accuracy*** of the measurement (i.e. how close the measurement is to the real value). Precision errors are related to the measurement conditions and are random in nature (i.e. they can be treated statistically and can be evaluated by performing several measurements).

In this section we evaluate measurement errors in corneal aberrations methodology and refer to errors in total aberrations as reported in previous works.

5.1 Bias errors: Accuracy

The accuracy of the laser ray tracing technique to measure total aberrations has been tested by comparing results with two other total aberration measurement techniques, a Hartmann-Shack sensor and a spatially resolved refractometer[3]. An average global standard deviation in Zernike coefficients across techniques was reported to be 0.09μm.

Bias errors in corneal aberrations methodology are induced by the following factors:

1) ***Errors associated with the reflection Placido disk technology and the reconstruction algorithm.***

Extensive work has been done previously to test the accuracy of videokeratoscopes and even ANSI standards have been proposed with protocols for accuracy testing[36].

Several studies have analyzed the accuracy of the measurement of Placido disk systems[23, 37, 38] on test surfaces. All these studies evaluate these errors as the differences in the elevation data provided by the videokeratoscope with respect to ***reference values*** on the same surfaces measured with profilometric or interferometric techniques, assuming that bias errors of these reference values are negligible with respect to those from the videokeratoscope.

We performed measurements of elevation data on a PMMA 8-mm sphere before and after laser ablation (using the same laser system used for refractive surgery, for a 3 D correction over a 6 mm optical zone). As it will be seen in chapter V, this procedure is expected to change the curvature and asphericity of the treated surface. We compared surface elevation measured with the videoqueratoscope with two other standard techniques: A Talysurf system based on contact profilometry and a confocal scanning microscope (Sensofar PLμ). The three systems measured spherical surfaces of 8.01 mm before treatment (the nominal value was 8.00 mm). The elevation results after the laser ablation procedure are shown in Figure II.9 A. The differences between techniques increase with the radial coordinate, and at the center. Measurements with the confocal microscope are limited only to a region of 2mm of radius. Because of this, we only considered as reference values those given by the Talysurf. The maximum absolute difference between Talysurf and videokeratoscope techniques was 1.77 μm and the average error given by the root mean square error (RMSE) was 0.724 μm.

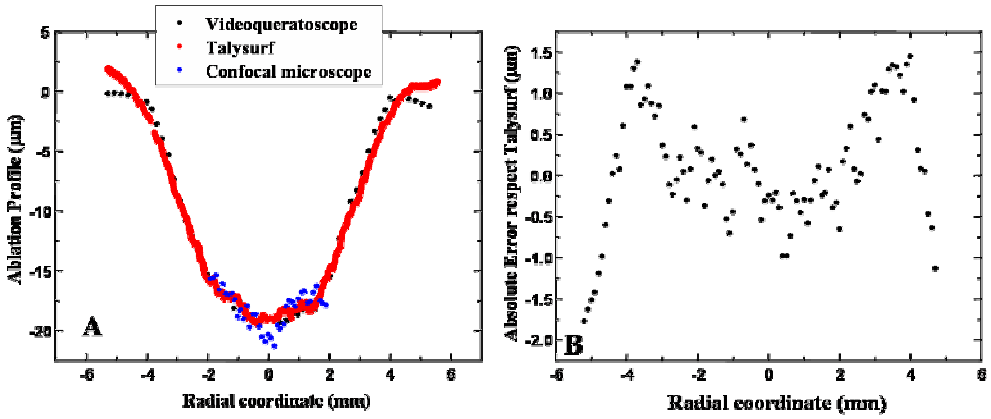

Figure II.9: A) Elevation raw data subtracted from a PMMA treated sphere, in a random meridian. Data from the confocal microscope are given in a smaller area because of the range limitation of the device. **B)** Videokeratoscope elevation data minus Talysurf elevation data (absolute errors). Videokeratoscope data have been interpolated over an equi-spaced sample to allow appropriate comparison.

Previous studies measuring accuracy in Humphrey videokeratoscope also report a decrease in the accuracy with radial distance of the surface point[23, 38], although higher errors have been reported, RMSE of 3.7 µm for a 5.4 mm radius conic surface in Schultze's study[38] and RMSE within 1-3 µm in an ellipsoidal surface (R=9.37 mm, Q=0.6) in Guirao et al[23]. The error distribution in both studies is given graphically. Shultze (Figure 1, pag 102)[38] found (for conic surfaces) an elevation error that increases slightly up to 2.4 mm of radial coordinate and then increases following a linear relation with positive absolute errors, thus meaning an over-estimation. Guirao & Artal also found (Figure 3, pag 960)[23] a linear increase in the error with radial coordinate (information in the sign is not provided) but much lower than the one found by Schultze. The distribution of error found in our study is shown in figure II.9.B). There appears to a linearly increasing error towards positive values with radial coordinate, although this pattern changes beyond 4 mm from the center.

2) Errors in surface modeling

As mentioned above, corneal elevation maps are fitted to a Zernike polynomial surface. The goodness of this representation can be evaluated as the difference between the raw elevation data and the fitted elevation data. Figure II.10 shows absolute differences (Raw height data – Fit height data) for an individual cornea.

The largest difference found across the cornea was 2 µm. Fit differences in each ring present a random distribution, but with increasing radial coordinate errors values increase. For ring #1 (~0.4 mm from the center) the data show an absolute fit difference of 0.398±0.345µm, while for ring #21 (~5 mm) that value is 0.704±0.569µm. This finding parallels the increasing experimental error of the videokeratoscope in peripheral data.

The Root Mean Square Error (RMSE) is used as general metric to evaluate the global goodness of the fitting. For a set of normal corneas (14 eyes) we obtained a mean RMSE of 0.43±0.11µm and for a set of post Lasik corneas (14 eyes) we measured 0.53±0.11µm.

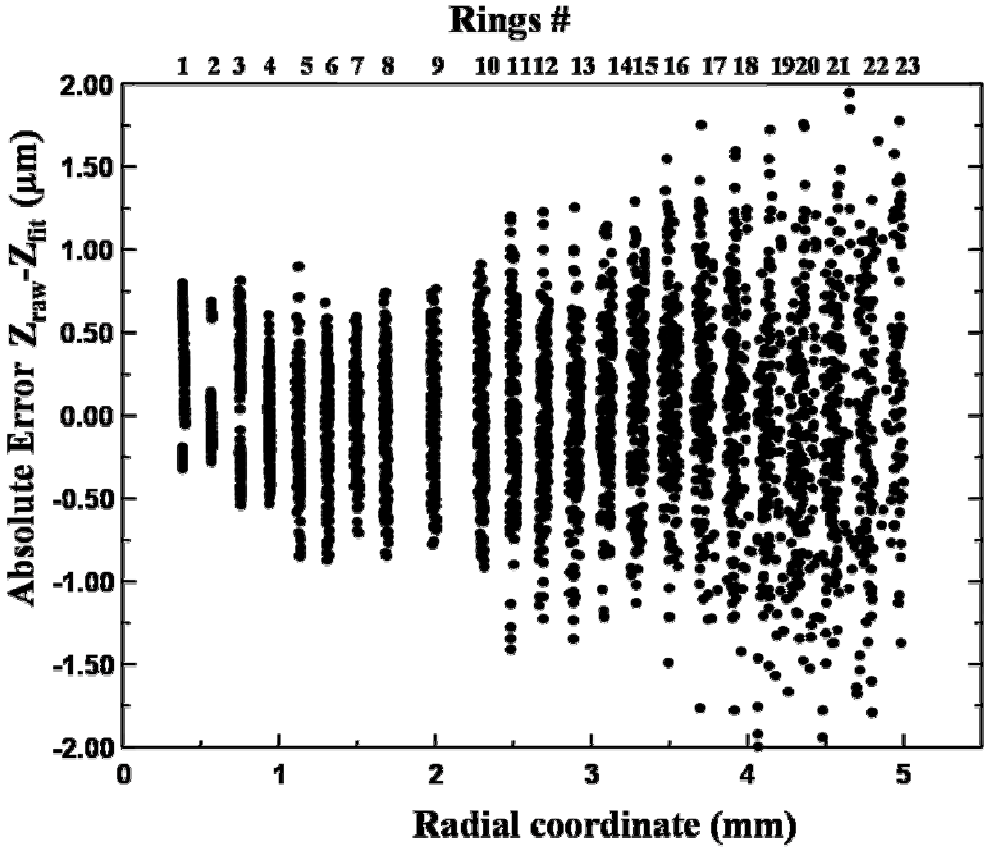

Figure II.10: Absolute differences (Raw height data – Fit height data) as function of radial coordinate for an individual cornea.

The RMSE can decrease slightly using more terms in the Zernike polynomial fitting. However, it has been demonstrated that increasing the order of the expansion may result in capturing higher amounts of experimental error of the videokeratoscope. Iskander has demonstrated that a high number of Zernike terms is not necessary for an accurate fitting of corneal data [19]). We typically use a 7th order Zernike expansion with 35 terms to fit corneal elevation data, as we do to describe the total wave aberration.

3) Propagation of videokeratoscope bias error to wave aberration estimation

To evaluate the propagation of videokeratoscope bias error onto the wave aberrations, we have simulated different elevation data errors and calculated differences in corneal aberrations estimation. A first approach is to estimate the propagation error as the multiplication of the refractive index differences by the root mean square bias error of elevation data[37]. However this approach does not consider the spatial distribution of

elevation error and the "smoothing" effects that surface modelling with a Zernike polynomial expansion performs over the elevation error. Therefore, that approach tends to overestimate the propagation error. It is clear that the distribution of elevation errors plays an important role in the error propagation to the wave aberration estimation. As mentioned above, different studies provide different distributions and magnitudes of the errors of the elevation data. We used the highest value available (RMSE=3.7μm) as well as the value found in our study (RMSE= 0.724μm) to evaluate the range of possible error for the wave aberration estimation.

We simulated two different error distributions and their final effect on aberrations errors: 1) A random distribution error across radial coordinates. 2) A linear increasing error with radial coordinate.

Results are shown in Table II.3, where the RMS and standard deviation value of the wave aberration residuals (differences between estimation with and without simulated error), provides an average bias wave aberration error. Given the properties of the Zernike polynomials, the RMS of the wave aberration residual divided by the square of the number of Zernike coefficients is an estimate of the mean standard deviation error of the Zernike coefficients (standard error).

	RMSE of elevation data = 3.7 μm		RMSE of elevation data = 0.724 μm	
	RMS residual wavefront (μm)	Mean standard error of Zernike coefficients	RMS residual wavefront (μm)	Mean standard error of Zernike coefficients
Random distribution	0.0874	0.0152	0.0171	0.0030
Linear distribution	0.1061	0.0185	0.0206	0.0036

Table II.3: Propagation of bias error in elevation data to wave aberration error for the corneal topography of a highly aberrated eye (RMS wavefront error=2.1849 μm). Simulation with an elevation RMS error of 3.7 μm (as reported by Schultze et al.) and 0.724 μm (from this study) assuming both a random and a linear distribution of the error

These results indicate that a random error induces a lower error than a systematic linear error in the estimation of the wave aberration. From the above simulations we can estimate a range of error (mean standard error of Zernike coefficients) of 0.0036-0.0185 μm, with a median value of 0.013 μm. It should be noted that these results are obtained from the error associated to a specific profile in PMMA, and simulating a determined

error distribution over a particular high aberrated cornea. Different results may be obtained for different elevation profiles or error distribution. However our results are obtained in an extreme case: a profile produced by a LASIK ablation; therefore with simpler profiles, such as no treated corneas, the errors are probably lower.

5.2 Precision errors

Precision errors are generated by changes in the measurement conditions.

In total aberrations measurements the precision was evaluated by estimating the Zernike standard deviation averaged across terms. We found that it ranged from 0.01 µm to 0.12 µm depending on the study (see different chapters for specific values).

In the corneal aberration measurements the sources of precision errors include defocusing of the rings captured by the camera, misalignment between the videoqueratographer axis and corneal axis (axis passing through the center of curvature of the anterior corneal surface and normal to the surface), microfluctuations in eye position [b], tear film fluctuations, or different effects of the eyelid, These type of errors can be treated statistically and its effects evaluated by performing consecutive measurements.

Figure II.11 shows the distribution of standard deviation in elevation data measurement of the videokeratoscope in 5 consecutive measurements on the same cornea used for the simulations of accuracy propagation.

The standard deviation increases with radial coordinate with a mean value of 2.23±2.11 µm. This variability in the surface elevation measurements results in the variability of corneal Zernike coefficients shown in Figure II.12. The mean standard deviation across Zernike terms of is 0.015±0.0236 µm.

[b] Buehren et al[39] have proposed some techniques to minimize errors associated to microfluctuations in eye position such as tilts or shifts but requiring taking multiple measurements within a short time period.

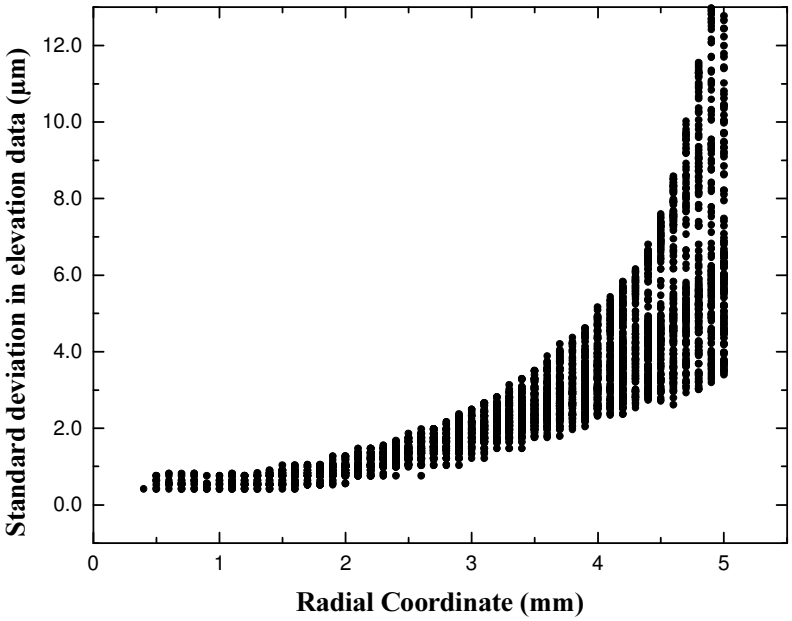

Figure II.11: Standard deviation in elevation data (µm) measurement of the videokeratoscope across five consecutive measurements on the same cornea as function of radial coordinate (mm).

5.3 Combining bias and precision errors

The combination of bias and precision errors provide the actual errors of the technique and permits comparison with other aberration techniques. The global error is given by the addition of both bias and precision errors (assuming no interrelation of both type of errors). It is interesting to point out that the standard error (averaged across Zernike coefficients) due to accuracy (0.013 µm) is of the same order than that due to precision (0.015 µm). These errors of corneal aberration measurements with the described methodology are lower than those found for total aberration across Zernike terms using Laser Ray Tracing (0.063 µm).

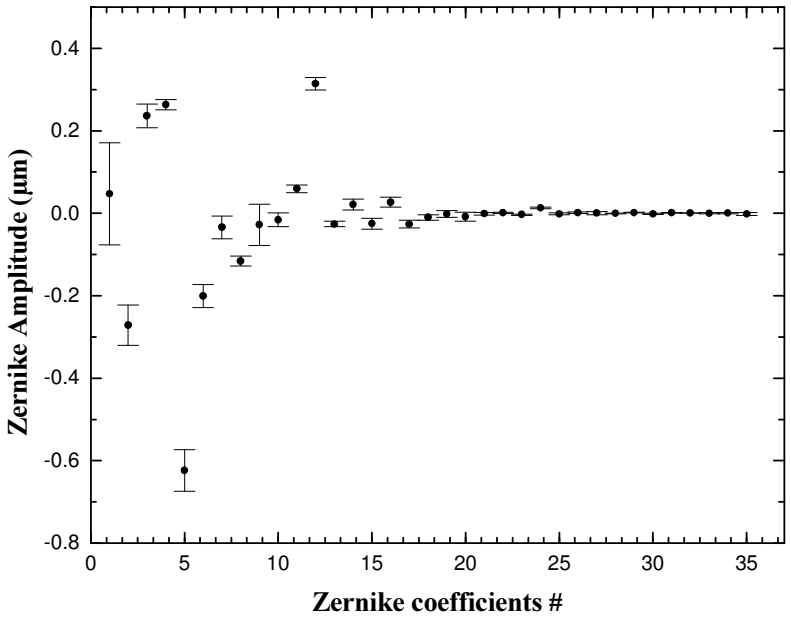

Figure II.12: Standard deviation in Zernike wave aberration coefficients (µm) across five consecutive measurements on the same cornea.

5.4 Errors in internal aberration estimation

Internal aberrations are estimated by direct subtraction of corneal from total aberrations which are independent measurements. Therefore errors associated to internal aberrations measurement is estimated adding the errors from both techniques.

6. Software for corneal fitting and aberration computation

For the estimation of the corneal aberrations we have written codes in different programming languages. Modelling of the corneal surface from videokeratoscope data and shift correction are written in Matlab. Virtual ray tracing through corneal surface were performed with Zemax macro language. A user-friendly Visual Basic global interface has been developed to perform the different steps to obtain corneal aberrations. This interface has a modular organization where each module performs a different task.

1) Generate Zemax files: To fit the videokeratoscope data to a surface shape

to be used in Zemax. Two input parameters: Corneal surface fitting diameter and the number of Zernike terms to be used in the polynomial fitting.

2) Conic fitting: To fit videokeratoscope data to a conic surface. Three input parameters: Corneal surface fitting diameter and the initial apex radius and asphericity to perform the fitting routine (an additional parameter, piston with no physical meaning, is also used).

3) Simulating ray tracing: To create the Zemax macro needed to perform the virtual ray tracing. Three input parameters: Wavelength, corneal surface diameter and the notation of the Zernike aberrations.

4) Corneal aberrations with respect to the pupil center. To correct the shift between pupil center and corneal reflex.

Figure II.13 shows the interface with its modules.

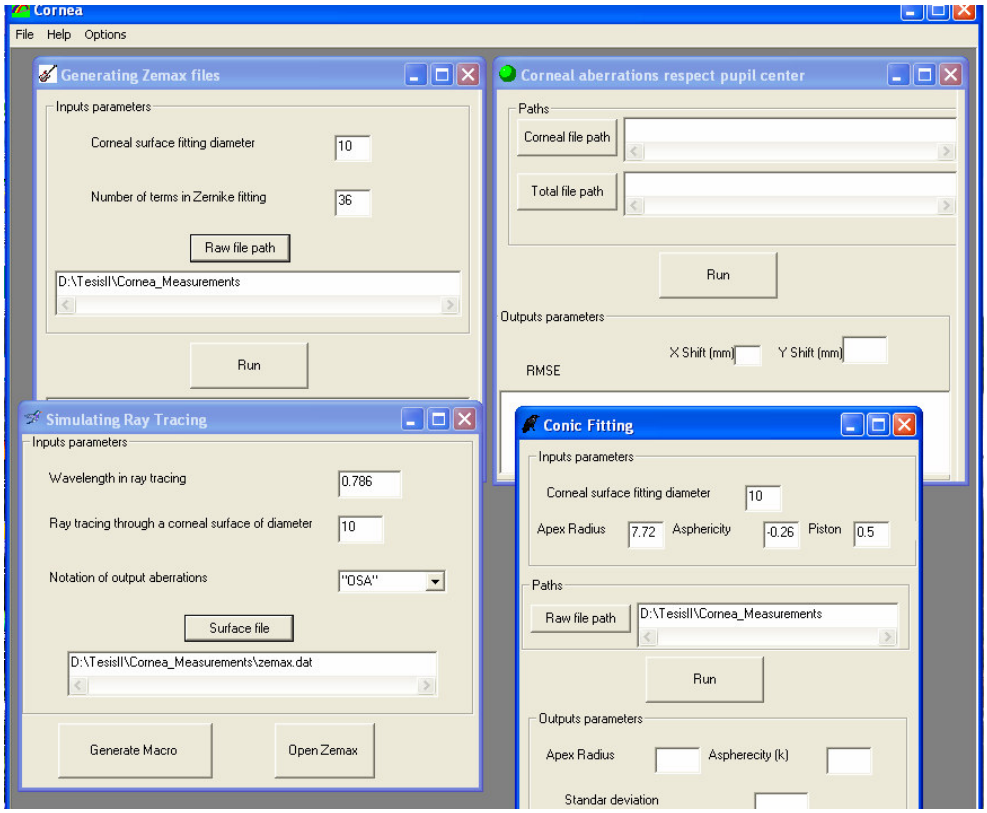

Figure 13: Interface written in Visual Basic of the software developed to evaluate corneal aberrations.

7. Protocols in subject measurements

The procedures involving subjects were reviewed and approved by Institutional Bio-ethical Committees of the Consejo Superior de Investigaciones Científicas, Instituto de Oftalmobiología Aplicada (Universidad de Valladolid) and Fundación Jimenez Diaz,Madrid, and met the tenets of the Declaration of Helsinki.

Each patient signed a consent form. All the measurements presented in this thesis were performed under pupil dilation (with 1 drop tropicamide 1%). A complete measurement of the total wave aberration, including informed consent explanation, pupil dilation and dental impression fabrication took less than 45 minutes.

In addition to total aberration and videokeratoscope other measurements were typically conducted on the patients: Axial length and anterior chamber depth with an optical biometer based on Optical Coherence Tomography (IOL Master, Carl Zeiss, Germany), autorrefraction (Automatic Refractor Model 597, Humphrey-Zeiss), and slit lamp examination.

All subjects in the present thesis are selected patients from the Instituto de Oftalmobiología de Valladolid (IOBA), from the Fundación Jimenez Diaz (FJD) Madrid or normal volunteers. All participating subjects had a previous eye examination in a clinic.

8. References

1. R. Navarro and M. A. Losada, "Aberrations and relative efficiency of light pencils in the living human eye," Optom Vis Sci 74, 540-547 (1997).
2. R. Navarro and E. Moreno-Barriuso, "Laser Ray Tracing versus Hartmann-Shack Sensor for Measuring Optical Aberrations in the Human Eye," J Opt Soc Am A 17, 974-985 (2000).
3. E. Moreno-Barriuso, S. Marcos, R. Navarro, and S. Burns, "Comparing Laser Ray Tracing, Spatially Resolved Refractometer and Hartmann-Shack Sensor to measure the ocular wave aberration," Optom Vis Sci 78, 152-156 (2001).
4. L. Llorente, L. Diaz-Santana, D. Lara-Saucedo, and S. Marcos, "Aberrations of the human eye in visible and near infrared illumination," Opt Vis Sci 80(1), 26-35 (2003).
5. R. Navarro and E. Moreno-Barriuso, "Laser Ray-Tracing versus Hartmann-Shack Sensor for Measuring Aberrations in the Eye," presented at the Technical Digest Opt. Soc. Am. Annual Meeting, Baltimore (USA), 1998.
6. S. A. Burns, J. McLellan, and S. Marcos, "Sampling effects on measurements of wavefront aberrations of the eye," presented at the Investigative Opthalmology and Visual Science, Fort Lauderdale, Florida, USA, 2003.

7. M. Born and E. Wolf, *Principles of Optics,* 6th ed. (Pergamon Press, Oxford, U.K., 1993).
8. X. Cheng, A. Bradley, X. Hong, and L. N. Thibos, "Relationship between refractive error and monochromatic aberrations of the eye," Optom Vis Sci 30(1), 43-49 (2003).
9. Z-136.1-1993, "American National Standar Institute. American National standar for the safe use of lasers," (Orlando, FL: The Laser Institute of America, 1993.).
10. D. V. Sharma, D. K. Shumar, and A. K. Ghatak, "Tracing rays through graded index media," Appl Opt 21, 984-987 (1982).
11. Y. Le Grand and E. Hage, *Physiological optics* (Springer-Verlag, Berlin, 1980).
12. I. Escudero-Sanz and R. Navarro, "Off-axis aberrations of a wide-angle schematic eye model," J Opt Soc Am A 16, 1-11 (1999).
13. R. Navarro, J. Santamaría, and J. Bescós, "Accommodation-dependent model of the human eye with aspherics," J.Opt.Soc.Am.-A 2, 1273-1281 (1985).
14. M. Herzberger, "Colour Correction in Optical Systems and a New Dispersion Formula," Optica Acta 6, 197-215 (1959).
15. B. Seitz, F. Torres, A. Langenbucher, A. Behrens, and E. Suárez, "Posterior corneal curvature changes after myopic laser in situ keratomileusis," Ophthalmology 108, 666-673 (2001).
16. C. Campbell, "Reconstruction of the corneal shape with the MasterVue Corneal Topography System," Optom Vis Sci 74, 899-905 (1997).
17. J. Schwiegerling, J. E. Greivenkamp, and J. M. Miller, "Representation of videokeratoscopic height data with Zernike polynomials," J Opt Soc Am A 12, 2105-2113 (1995).
18. D. R. Iskander and M. Collins, "Modelling of corneal surfaces with radial polynomials," IEEE Transactions on Biomedical engineering 49(4), 320-328 (2002).
19. D. R. Iskander, M. J. Collins, and B. Davis, "Optimal modeling of corneal surfaces with zernike polynomials," IEEE Trans Biomed Eng 48(1), 87-95 (2001).
20. T. O. Salmon, "Corneal contribution to the wavefront aberration of the eye," (Indiana, 1999).
21. V. N. Mahajan, *Optical imaging and aberrations: Ray geometrical optics* (SPIE-The International Society for Optical Engineering, Washington, 1998), Vol. 1.
22. R. Hemenger, A. Tomlinson, and K. Oliver, "Corneal optics from videokeratographs," Ophthal Physiol Opt 15, 63-68 (1994).
23. A. Guirao and P. Artal, "Corneal wave aberration from videokeratography: accuracy and limitations of the procedure," J Opt Soc Am A 17, 955-965 (2000).
24. H. C. Howland, J. Buettner, and R. A. Applegate, "Computation of the shape of normal corneas and their monochromatic aberrations from videokeratometric measurements," OSA Tech. Digest Series Vis. Sci & Its Appl 2, 54-57 (1994).
25. J. Schwiegerling and J. E. Greivenkamp, "Using Corneal height maps and polynomial decomposition to determine corneal aberrations," Optom Vis Sci 74, 906-916 (1997).
26. E. J. Sarver and R. A. Applegate, "Modeling and predicting visual outcomes with VOL-3D," J Refract Surg 16, S611-S116 (2000).
27. J. E. Greivenkamp, J. Schwiegerling, J. M. Miller, and M. D. Mellinger, "Visual acuity modeling using optical raytracing of schematic eyes," Am J Ophthalmol 120, 227-240 (1995).
28. J. J. Camp, L. J. Maguire, B. M. Cameron, and R. A. Robb, "A computer model for the evaluation of the effect of corneal topography on optical performance," Am J Ophthalmol 109, 379-386 (1990).
29. S. Patel, J. Marshall, and F. Fitzke, "Refractive index of the human corneal epithelium and stroma," J Refract Surg 11, 100-106 (1995).
30. J. Prydal and F. Campbell, "Study of precorneal tear film thickness and structure by interferometry and confocal microscopy," Invest. Ophthalmol. Vis. Sci. 33(6), 1996-2005 (1992).
31. C. Albarrán, A. M. Pons, A. Lorente, R. Montés, and J. M. Artigas, "Influence of the tear film on optical quality of the eye," Contact Lens and Anterior Eye 20(4), 129-135 (1997).
32. P. Vinciguerra, F. I. Camesasca, and A. Calossi, "Statistical analysis of physiological aberrations of the cornea," J Refract Surg 19(2 Suppl), S265-269 (2003).
33. L. Wang, E. Dai, D. D. Koch, and A. Nathoo, "Optical aberrations of the human anterior cornea," J Cataract Refract Surg 29, 1514-1521 (2003).
34. S. Marcos and S. A. Burns, "On the symmetry between eyes of wavefront aberration and cone directionality," Vision Res 40, 2437-2447 (2000).
35. R. B. Mandell, C. S. Chiang, and S. A. Klein, "Location of the major corneal reference points," Optom Vis Sci. 72, 776-784 (1995).

36. S. A. Klein, "Corneal topography: A review, new ANSI standars and problems to solve," presented at the OSA Trends in Optics and Photonics, Washington DC, 2000.
37. R. A. Applegate, R. B. Nuñez, J. Buettner, and H. HC, "How accurately can videokeratographic systems measure surface elevation.," Optom Vis Sci 72, 785-792 (1995).
38. R. L. Schultze, "Accuracy of corneal elevation with four corneal topography systems," J Refract Surg 14, 100-104 (1998).
39. T. Buehren, B. J. Lee, M. J. Collins, and D. R. Iskander, "Ocular microfluctuations and videokeratoscopy," Cornea 21(4), 346-351 (2002).